Liquid Crystalline Pressure-Sensitive Adhesive based on a Shape-Assisted Molecular Assembly with Electron-Deficient Twofold Columnar π-Stacking

Kota Ono, Kensuke Suga, Mitsuo Hara, Katsuki Miyokawa, Tsubasa Honda, Kazuya Otsubo, and Shohei Saito*

KEYWORDS: Liquid Crystal, Supramolecule, π-Stacking, Adhesive

ABSTRACT: Recently, the chemistry of supramolecular adhesives has rapidly progressed in materials science and tissue engineering. Many structural motifs with a variety of non-covalent interactions have been proposed for advanced adhesive properties. Here, we propose a new materials class of liquid crystalline pressure-sensitive adhesive (LC-PSA). Without the aid of hydrogen bonding or Coulomb force, a cyclooctatetraene(COT)-fused electron-deficient dipyridophenazine dimer (dppz-FLAP) forms a tight twofold columnar π-stacking based on its V-shaped molecular structure (π-π distance: 3.32 Å). With the dppz-FLAP core as a mesogen of liquid crystal, a high shear LC-PSA bearing a well-defined packing structure in a hexagonal columnar phase has been developed. Both hydrophobic and hydrophilic glass substrates can be easily bonded at room temperature by simply pressing a flake sample of the molecular adhesive between the substrates. Tensile shear strengths reached approximately 1 MPa for glass, SUS and Fe substrates based on dispersion interaction with significant ductility, while the easy peelability on a PET tape was confirmed. The rigid columnar structure formed by the shape-assisted assembly results in the high cohesive force of the material, while the soft liquid crystalline properties provide sufficient fluidity as a PSA. Viscoelastic analysis revealed a unique position of the LC-PSA ($G'\sim10^7$ Pa, $G''\sim10^6$ Pa) compared with conventional PSAs. The concept of LC-PSA based on the rigid/soft hybridization and hydrogen-bond-free molecular engineering extends the potential of supramolecular adhesives and functional small-molecule materials.

INTRODUCTION

Supramolecular adhesives have emerged as a pioneering class of compounds in the broad and ever-evolving field of materials science and tissue engineering.[1–6] Unlike conventional polymeric adhesives, which rely on strong covalent bonds, supramolecular materials are formed by the network of non-covalent interactions such as hydrogen bonds, van der Waals force, and other electrostatic interactions (Figure 1a).[7,8] Due to the abundant types of non-covalent (or dynamic) bonds, supramolecular adhesives offer many advantages over conventional polymeric adhesives, including inherent self-healing[9] and reusable[10–13] properties, stimuli-responsive properties,[14–19] and improved bio-conformability.[20,21] These adhesives are composed of a variety of molecular motifs such as host-guest systems,[17,19,22–26] multiple hydrogen bonds,[27–35] disulfide bond,[9,36] coordination complexes,[37–39] Pt-Pt interactions,[40] and eutectogel.[41] In particular, catechol analogs,[38,39,42–46] ionic liquid motifs,[42,47,48] and nucleobase pairs[49,50] offer characteristic functions in universal adhesion, small-molecule adhesion, and high shear strength (~16 MPa), respectively. To enhance the toughness of adhesives, energy dissipation by weak bond breaking has been also focused in recent studies.[51] On the other hand, unambiguous characterization of their packing structures has been limited due to the non-uniform, less directional supramolecular assemblies, which hinders precise mechanistic studies.

Liquid crystals (LCs) possess a unique position in materials science.[52–54] In addition to the characteristic features of structural anisotropy, controllable optical/mechanical properties, and electric field response, the packing structures of molecular LCs can be clearly analyzed, making it easy to discuss structure-property relationships.[55,56] We have previously reported an LC adhesive with a photoinduced melting function,[57] but the development of LC adhesives is still in its infancy, whereas the above-mentioned supramolecular adhesives are flourishing. The strength of intermolecular interactions in LCs varies largely depending on the LC phase. Nematic and smectic LCs are not suitable for adhesive materials because the fluidity of these phases is too high to exhibit sufficient cohesive force. In contrast, we have found that a columnar liquid crystal based on a characteristic twofold π stacking structure of a V-shaped molecule (see below) produce high cohesive force.[57] Self-assembly based on the appropriate shape of such nonplanar molecules (including saddle-shaped[58–62] or bowl-shaped ones[55,63–66]) has attracted attention as "shape-assisted self-assembly" in recent years. In particular, to construct mechanically rigid self-assembly structures with less directional "π-stacking interaction",[67] it is essential to design molecules with folded shapes because it works as rotational locks that can geometrically restrict the translational and rotational components of motion between building blocks.[58]

However, the LC adhesive still suffers from a common limitation, which is shared with supramolecular adhesives. That is, most of these materials require a hot-melt process for the adhesion process. The pre-heating process limits their use and poses a challenge particularly in the adhesion with thermoplastic substrates. To overcome this problem, reversible photo-switching process has been recently proposed, using azo components and so on.[68–73] In these studies, the adhesion for coverage of substrate surfaces is triggered by the photoinduced melting of materials, and the subsequent curing is induced by a different wavelength of light. On the other hand, the advanced photomelting process has another serious limitation in that the

substrates must be transparent for penetration of the excitation light. In this context, the simple adhesion function without heat or light, like pressure-sensitive adhesives (PSAs), is the next important challenge. While polymer-based PSAs have been classically developed,[74–78] only a few emerging examples have been reported as supramolecular PSAs[79–82] and, to the best of our knowledge, liquid crystalline PSA (LC-PSA) has not been developed.

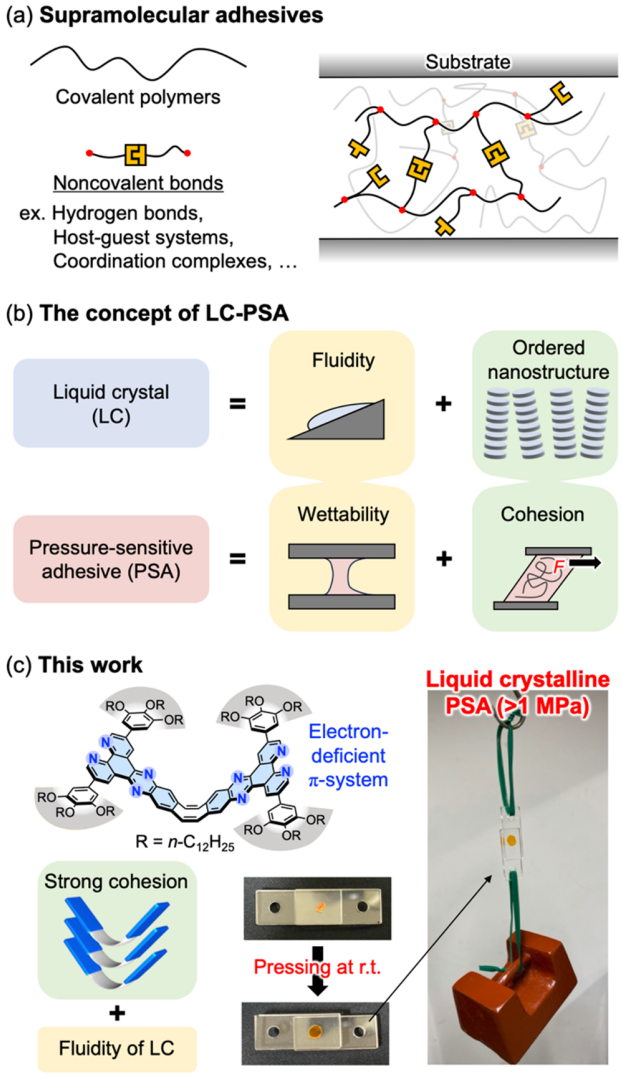

Figure 1. (a) Schematic illustration of supramolecular adhesives. (b) Similarity between LCs and PSAs. (c) A small-molecule LC-PSA reported in this work.

Here we report the development of a novel LC-PSA with sufficient cohesive strength. In general, PSA requires a delicate balance between two seemingly contradictory properties: wettability, which allows the adhesive to spread over the substrate surface, and cohesion, which prevents internal disruption of the material (Figure 1b). We focused that these properties have similarities to those of columnar LCs. They exhibit a combination property of fluidity, akin to liquids, and an ordered nanostructure, characteristic of crystals. Inspired by this idea, we hypothesize that a columnar LC with the shape-assisted self-assembly may serve as a high shear LC-PSA without the aid of hydrogen bonds or Coulomb force.

In this work, we have designed a cyclooctatetraene (COT)-fused dipyridophenazine (dppz) dimer, called dppz-FLAP. The series of flapping molecules (FLAPs), which are characterized by V-shaped or saddle-shaped structures due to the central COT ring, provide a good example of the shape-assisted self-assembly, unless steric hinderance is present.[61,62,83,84] The V-shaped molecules are spontaneously stacked to form tight twofold columnar π-stacking with optimal dihedral angles of the bent COT conformation (Figure 1c). Nitrogen atoms at the pyrazine and pyridine rings leads to the electron-deficient properties of the dppz wings.[85] The extended π-skeleton with high electron deficiency induce more tight π-stacking due to strong van der Waals attraction and less electronic repulsion.[86–88] The unique twofold columnar as-sembly of the FLAP mesogen further enhances intermolecular interaction, leading to strong cohesive force of materials. On the other hand, by introducing multiple long alkyl chains into the dppz-FLAP mesogen, we aimed to form a columnar LC phase at room temperature and develop a LC-PSA with sufficient wettability under pressure.

RESULTS AND DISCUSSION

Gram-Scale Synthesis of the Liquid Crystalline PSA

Prior to the preparation of the LC compound, parent dppz-FLAP with no peripheral substituent, **dppz-FLAP0** was synthesized (Figure 2a). The condensation reaction[89–92] of the precursors, dibenzo[*a*,*e*]cyclooctatetraene-2,3,8,9-tetraamine hydrochloride **1**[91] and 1,10-phenanthroline-5,6-dione **2**, was conducted in MeOH, providing **dppz-FLAP0** in 87% yield. The solid sample of **dppz-FLAP0** allowed unambiguous structural characterization of the twofold columnar π-stacking by powder XRD analysis (Figure 3a).

On the other hand, liquid crystalline dppz-FLAP bearing four 3,4,5-tris(dodecyloxy)phenyl substituents, **dppz-FLAP1** was synthesized on a gram scale in a three-step procedure starting from previously reported compounds. Suzuki-Miyaura cross-coupling reaction of the protected phenanthroline **3** and the arylboronic acid provided the phenanthroline derivative **4** in 37% yield. Subsequent deprotection to **5** and the condensation of **5** with **1** afforded **dppz-FLAP1** in 65% yield for these two steps. With this reaction scheme, 1.0 g of **dppz-FLAP1** was obtained. The solubility of **dppz-FLAP0** was quite low because of the lack of substituents to improve solubility. Therefore, the NMR analysis of **dppz-FLAP0** was performed in a protonated form in a TFA-*d* solution. In contrast to **dppz-FLAP0**, **dppz-FLAP1** was highly soluble in common organic solvents due to the multiple dodecyl groups, while practically no solubilities in water and methanol were confirmed. The flake sample of **dppz-FLAP1** was obtained by precipitating from hot MeOH/toluene solution, and then drying the precipitate under vacuum at 90 °C (Figure 2b).

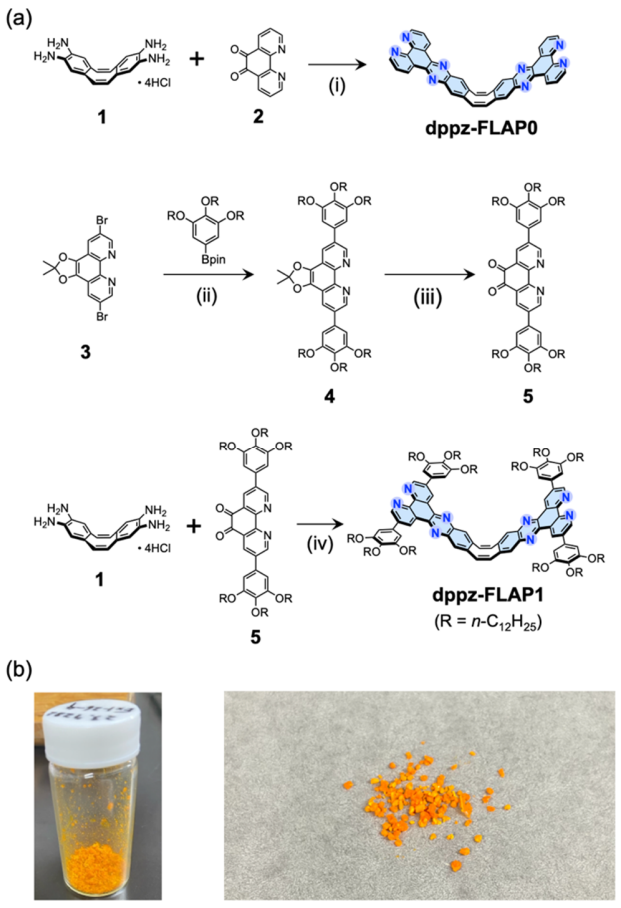

Figure 2. (a) Synthesis of COT-fused dppz dimers **dppz-FLAP0** and **dppz-FLAP1**. Conditions: (i) MeOH, 60 °C, 2 h, 87%; (ii) SPhos, $Pd_2(dba)_3$, Cs_2CO_3, dioxane/water (50:3), reflux, 63 h, 37%; (iii) TFA/water (30:1), 70 °C, 21 h, 88%; (iv) $CHCl_3$/MeOH (1:1), 60 °C, 22 h, 65%. (b) Photographs of **dppz-FLAP1** in a flake form.

Densely π-Stacked Columnar Structure with Shape and Electron Design

To investigate the strong intermolecular interaction between **dppz-FLAP0** molecules, we attempted X-ray crystallographic analysis, but only fine needle crystals were obtained. Therefore, we performed powder X-ray diffractometry (XRD) on the needle **dppz-FLAP0** crystals. The crystal structure was solved and refined through the Rietveld analysis[93] (Figures 3a and S6-1). The analysis showed the characteristic twofold columnar π-stacking structure of **dppz-FLAP0**, and the interfacial distance between the two dppz sites was determined to be 0.332 nm. Notably, this interfacial distance was shorter than that of the previously reported COT-fused anthracene dimer (0.350 nm),[57] indicating that **dppz-FLAP0** forms a more densely packed columnar structure compared to the conventional FLAP series.

By a computational method of independent gradient model based on Hirshfeld partition (IGMH),[94] the effective van der Waals interaction between the stacked dppz moieties was revealed in the columnar structure of **dppz-FLAP0** (Figure 3b). Furthermore, the effect of nitrogen doping was investigated by comparing the electrostatic potential maps in the density functional theory (DFT) analysis (Figure S11-2). The calculations showed that the increased number of doped nitrogen atoms made the π-skeleton more electron deficient. These results support the prediction of diminished electrostatic repulsion in the twofold columnar π-stacking, leading to the more rigid structural motif.

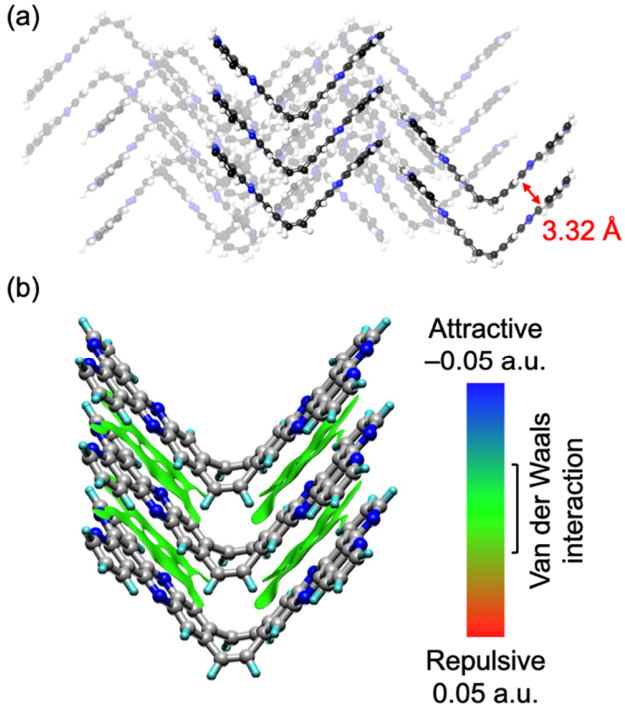

Figure 3. (a) Refined crystal structure of electron-deficient **dppz-FLAP0**. The interfacial distance between the dppz sites: 3.32 Å. Needle crystals of **dppz-FLAP0** were obtained by repeated recrystallization from a hot chlorobenzene solution. (b) IGMH for **dppz-FLAP0** mapped with colored isosurface for δg^{inter} = 0.005 a.u. The color scale for the mapped function sign(λ_2)ρ is –0.05 < sign(λ_2)ρ < 0.05.

Columnar LC Phase at Room Temperature

Before exploring the potential application of **dppz-FLAP1** as a material, the LC properties and phase transition behavior of **dppz-FLAP1** has been studied. In the differential scanning calorimetry (DSC) analysis of **dppz-FLAP1**, at least two characteristic phase transition peaks were observed during both the cooling and heating processes, i.e. the exothermic peaks at 1 °C and 208 °C during cooling and the endothermic peaks at 4 °C and 215 °C during heating (Figure 4a). Thermogravimetric analysis (TGA) showed almost no weight loss of **dppz-FLAP1** below 250°C (Figure S3-1). Although **dppz-FLAP1** was obtained in the flake form, polarized optical microscope (POM) observations revealed that shearing of the **dppz-FLAP1** sample at room temperature resulted in an anisotropic molecular alignment (Figure 5a), suggesting an LC phase at room temperature. The phase transition at 215 °C in the heating process was further investigated using variable-temperature POM observations.

As a result, an LC-to-isotropic liquid phase transition was observed between 180 °C and 218 °C (Figure S4-1). To gain insights into the phase transition around 0 °C, temperature dependent viscoelasticity measurements of **dppz-FLAP1** were performed (Figure S5-1). The storage modulus (G') and loss modulus (G'') of **dppz-FLAP1** increased near 0 °C with decreasing temperature. This indicated that the phase transition at 1 °C is likely to be an LC-to-solid phase transition in the cooling process.

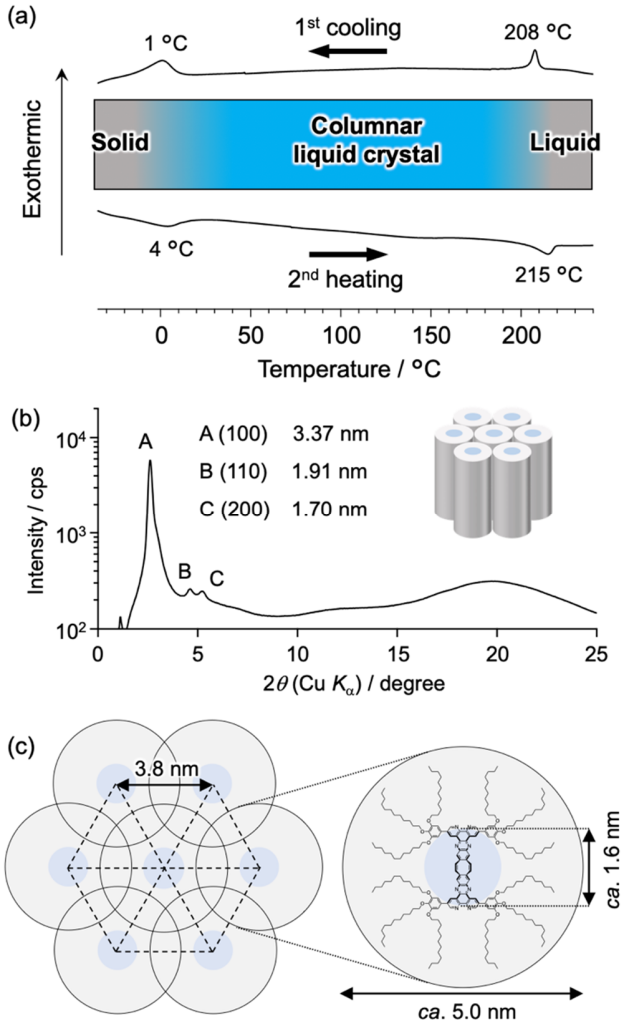

Figure 4. (a) DSC traces of **dppz-FLAP1** at 5 °C/min rate of cooling (top) and heating (bottom). (b) 1D XRD pattern of **dppz-FLAP1** at room temperature. (c) Plausible packing structure of the stacked **dppz-FLAP1** columns in the LC phase. The repeating cell unit is composed of the columnar array structure.

The structure of the LC phase was determined by the XRD pattern of **dppz-FLAP1** at room temperature. Three characteristic peaks observed at d = 3.37 nm as peak A (100), 1.91 nm as peak B (110), and 1.70 nm as peak C (200) supported a hexagonal columnar phase (Col_h) at room temperature (Figure 4b). The distance between the two column centers was calculated to be 3.84 nm, which corresponds to the estimated size of the bent **dppz-FLAP1** molecules with significant interdigitation of peripheral aliphatic chains (Figure 4c). The XRD patterns at 130 °C and 170 °C showed three additional peaks D, E, and F, which corresponds to (220), (310), and (400) planes, respectively (Figure S7-1). Hexagonal symmetry implies rotationally averaging dynamics of each columnar structure. These six peaks at 170 °C were sharper than those at 130 °C, and the peaks D, E, and F eventually disappeared by cooling to 25 °C. The blunting of these peaks suggested that short range order was lowered by reduced averaging dynamics.

Polarized optical microscopy (POM) observation of the sheared **dppz-FLAP1** sample suggested oriented columnar arrays (Figure 5a). To verify the column orientation after shearing, two-dimensional grazing incidence XRD (2D-GIXRD)[95] on the sheared sample was performed (Figure 5b). When the X-ray was irradiated from the perpendicular direction to the shearing, the (100) diffraction became more significantly anisotropic in the 2D pattern, while the parallel irradiation led to a less anisotropic diffraction (Figures 5c and 5d). This result indicates that the sheared columns are oriented parallel to the shear direction with edge-on arrangement on the substrate surface (Figure 5e).

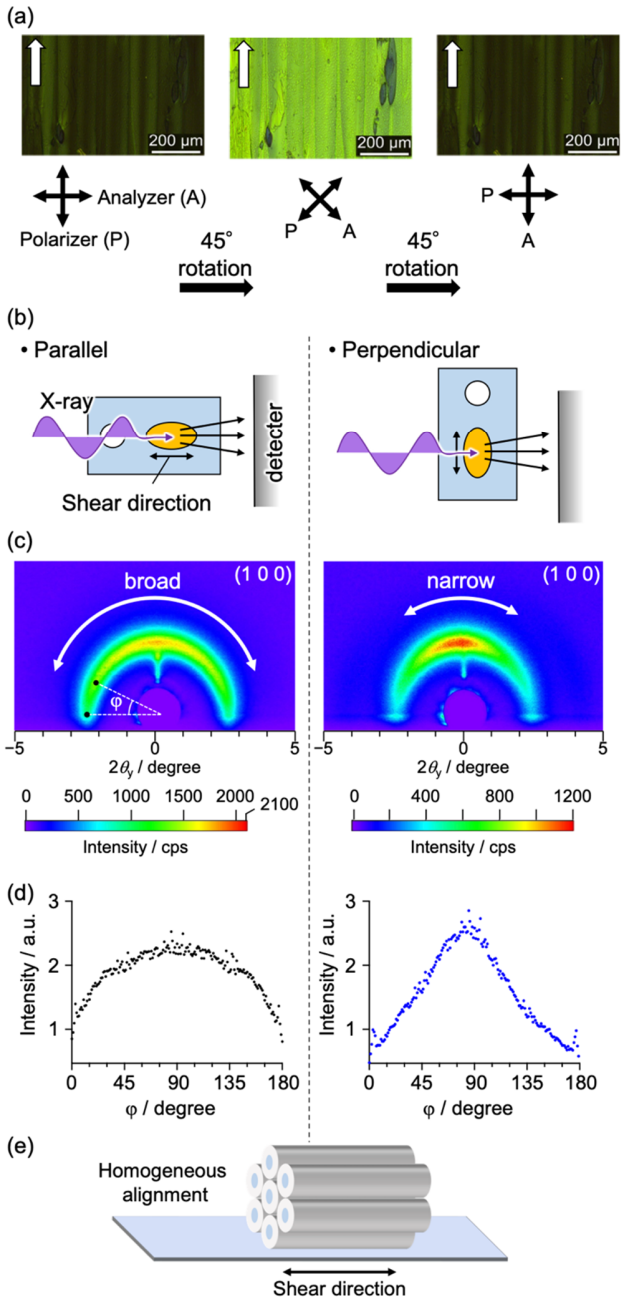

Figure 5. (a) POM images of a film of **dppz-FLAP1** sheared at room temperature. Shear was applied in the direction of a white arrow at room temperature. Double-headed arrows indicate the relative directions of the polarizer and analyzer. Three POM images of **dppz-FLAP1** were obtained by rotating the polarizer and analyzer 45° and 90° clockwise. (b) Schematic illustration of the 2D-GIXRD measurement from the top view. The X-ray and shear directions are parallel in the left figure and are perpendicular in the right figure. (c) 2D-GIXRD pattern of **dppz-FLAP1** after shearing at room temperature. (d) Azimuth angular (φ) dependence of the (100) diffraction intensity, obtained by converting the 2D-XRD images in (c). Intensity is calibrated based on the sample length (see Figure S8-1). (e) Estimated edge-on alignment of the columnar arrays after shearing.

Pressure-Sensitive Adhesion on Glass Substrates

When we applied shear stress to the **dppz-FLAP1** sample to investigate the LC properties, considerable force was required to initiate the shear. This interesting property prompted us to investigate the possibility of using **dppz-FLAP1** as a PSA (Supporting Movie 1). To evaluate the adhesive properties of **dppz-FLAP1**, samples for shear testing were prepared by placing ~3 mg of **dppz-FLAP1** between the hydrophilic glass substrates and applying a force of 150 N for 60 s to promote adhesion (Figure 6a). In the shear tests, the **dppz-FLAP1** sample exhibited a maximum strain of 1.2 ± 0.1 MPa (Figure 6d, left). The stress-distance curve of the shear test showed characteristic creep behavior, and **dppz-FLAP1** can be classified as a strong and ductile adhesive (Figure 6c). After the shear test, the sample of **dppz-FLAP1** was remained on both two glass substrates, indicating typical cohesive failure. Since the appearance was almost preserved with a round shape (Figure 6b), we re-adhered the debonded specimens and measured the shear strength (Figure 6d, right). Due to the non-covalent interactions, shear strength was almost fully recovered (1.1 ± 0.2 MPa).

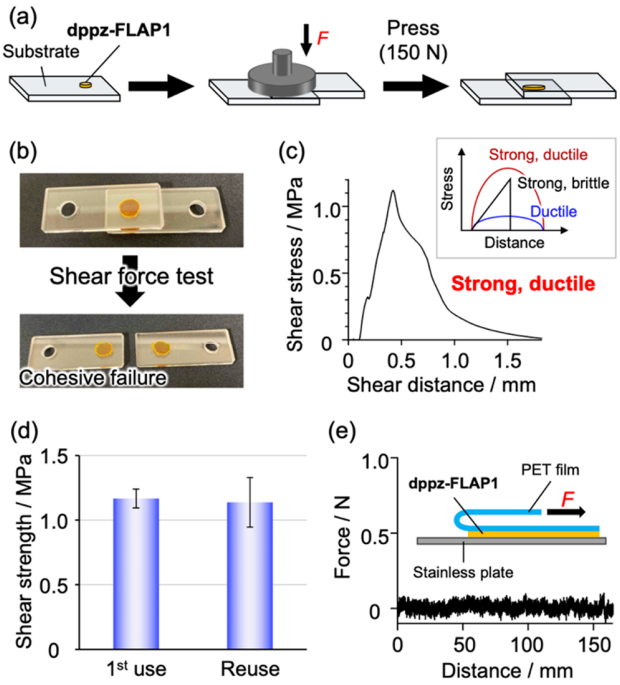

Figure 6. (a) Preparation of the specimen. (b) Photograph of the **dppz-FLAP1** specimen before and after the adhesion test. (c) Stress-distance chart of **dppz-FLAP1** in a shear test. The sample of **dppz-FLAP1** was sandwiched between hydrophilic glass substrates. The shearing rate was 1 mm/min. The classification of adhesive properties by stress-distance curves[51] is shown in the inset. (d) Shear strength of **dppz-FLAP1** put between two hydrophilic glass substrates. Shear strengths of the reused specimens were also shown. The error bars mean standard deviations. (e) Force-distance chart of **dppz-FLAP1** in the peeling test. The peeling rate was 30 mm/min. The film width was 10 mm.

In general, PSAs are also evaluated by peel and tack tests, in addition to shear tests. Therefore, we evaluated the peel and tack performance of **dppz-FLAP1**. Peel strength is an important parameter that indicates the force required to peel a tape from a solid surface at a constant rate per unit width of tape. In the peel test, **dppz-FLAP1** was applied to a 1 cm wide PET film, the PET film and stainless-steel plate were adhered to **dppz-FLAP1** by crimping, and the force required to peel it off was examined. Surprisingly, the tape could be easily peeled off with almost no force (Figure 6e). We also performed a probe tack test on **dppz-FLAP1**: a cylinder was adhered to a 0.37 mm thick **dppz-FLAP1** layer with a force of 1 N for 0.01 seconds, and the normal stress during the subsequent pull-up was monitored with a rheometer. Surprisingly, the maximum tack stress was measured to be 0.2 N (Figure S9-1), which is significantly lower than that of typical PSAs.[96] The significantly lower peel strength and tack stress could be attributed to the fact that **dppz-FLAP1** has almost no spinnability as a PSA. In short, these results emphasize that **dppz-FLAP1** has characteristic properties among PSAs, exhibiting resistance in the shear direction, but not in the peel and tack directions.

Definition of the LC-PSA in the Viscoelastic Window

It is known that viscoelasticity at low frequencies can explain wetting and creep behavior of the PSA, while viscoelasticity at high frequencies can explain peeling and quick-stick strength of the PSA. Therefore, the unique properties of **dppz-FLAP1**, such as high shear strength, easy peeling, and low tack strength, were investigated from the viscoelastic viewpoint using a rotational rheometer. Surprisingly, the storage modulus (G' = 1.0×10^7–1.5×10^7 Pa) and loss modulus (G'' = 1.2×10^6–1.4×10^6 Pa) of **dppz-FLAP1** were exceptionally high over the entire frequency spectrum (Figure 7a). From these moduli, the loss factor was calculated to be tan δ = 0.1, confirming the fully elastic behavior and low spinnability of **dppz-FLAP1** at room temperature. Notably, the G' values of **dppz-FLAP1** exceeded the Dahlquist criterion for a good PSA (G' ≤ 3×10^5 Pa).[97] In fact, **dppz-FLAP1** showed high creep resistance thanks to its high G' and tan δ, but because of the high G', a large force of 150 N was required to quickly wet the substrate. When the force was reduced to 50 N or 100 N, wetting was insufficient, and the adhesion area seemed to be small (Figure S10-1). These results suggest that the unique properties of **dppz-FLAP1** as a PSA are due to the combination of high G' and low tan δ. The extremely high storage modulus of **dppz-FLAP1** is presumably due to the tight columnar π-stacking structure of dppz-FLAP core and the large number of small van der Waals interactions between alkyl chains.

To define the position of **dppz-FLAP1** within the general PSA in terms of viscoelasticity, we used the concept of a "viscoelastic window" that classifies PSAs according to storage and loss moduli (Figure 7b).[98] As a result, **dppz-FLAP1** was classified as a high shear PSA in quadrant 2. The storage modulus of **dppz-FLAP1** was significantly higher and the area of the window of **dppz-FLAP1** was smaller than those of other common adhesives, such as cross-linked ploy(norbornene-*graft*-BE), poly(butyl acrylate-*co*-acrylic acid),[99] polymers synthesized from biobased monomers,[100] and thermoplastic polyurethanes[101] (comparison **1**–**4** in Figure 7c). For example, a high-shear PSA with high reusability and removability, developed by Kim (comparison **1**), has the maximum storage modulus of G' = 3×10^6 Pa at 100 rad s^{-1} and shear strength of 0.25 MPa,[102] which were lower than those of **dppz-FLAP1**.

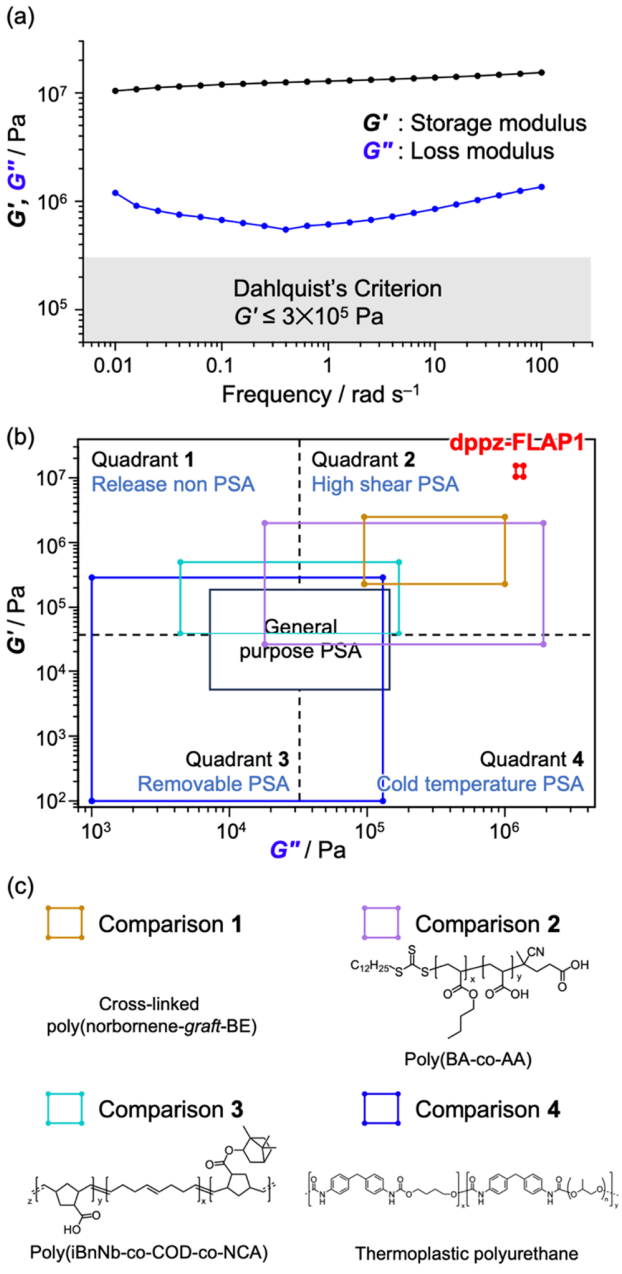

Figure 7. (a) Frequency dependence of storage modulus G' and loss modulus G'' of **dppz-FLAP1**. (b) Viscoelastic window and position of **dppz-FLAP1** within the window. (c) Chemical structure and storage and loss moduli of common PSAs. The viscoelastic window of the comparisons were referred as follows: comparison **1**,[102] **2**,[99] **3**,[100] and **4**.[101] BE : benzyl ether, BA : butyl acrylate, AA : acrylic acid, iBnNb : isobornyl norbornenate, COD : cyclo-1,5-octadiene, NCA : 5-norbornene-2-carboxylic acid.

Interpretation of the Adhesion Ability at the Interface between LC-PSA and Substrates

While the performance of **dppz-FLAP1** has been evaluated in terms of the cohesion property based on its viscoelastic properties, it is also important to evaluate adhesion force based on surface properties at the point of contact between the PSA and the substrates. To investigate surface properties in detail, contact angle and shear strength were measured on a variety of substrates. In addition to hydrophilic glass substrates, we used hydrophobic glass substrates, steel use stainless (SUS), iron (Fe), polyethylene terephthalate (PET), and polypropylene (PP) substrates. First, the contact angles between water or diiodomethane and **dppz-FLAP1** of the substrates were measured. These contact angles were converted into the dispersive and polar components of surface free energies (σ^d and σ^p) using Young's and Owens-Wendt's equations (Figure 8a).

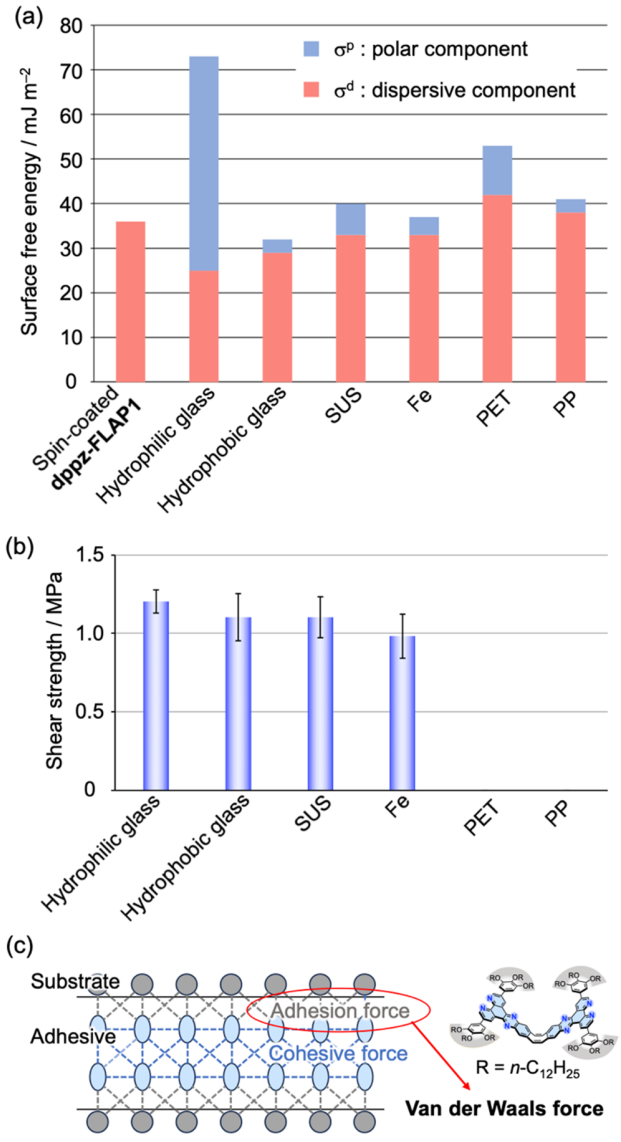

Figure 8. (a) Breakdown of the surface free energy of substrates and **dppz-FLAP1**. See Supporting Information for surface free energy calculations. (b) Substrate dependence of the shear strength. The error bars mean standard deviations. (c) Schematic illustration of adhesion by **dppz-FLAP1**.

As a result, σ^d and σ^p of the spin-coated **dppz-FLAP1** film were calculated to be σ^d = 36 mN/m and σ^p < 1 mN/m, respectively. Although σ^p did not vary much between substrates (σ^d = 25–42 mN/m), the value for σ^p varied greatly between substrates (σ^p = 3–48 mN/m). Despite the variety of σ^p between the substrates, the shear strengths did not change much between hydrophilic glass (σ^p = 48 mN/m, shear strength = 1.2 MPa), hydrophobic glass (σ^p = 3 mN/m, shear strength = 1.1 MPa), SUS (σ^p = 7 mN/m, shear strength = 1.1 MPa), and Fe (σ^p = 4 mN/m, shear strength = 0.98 MPa) substrates (Figure 8b). Unexpectedly, **dppz-FLAP1** hardly adhered to PET and PP substrates, and the shear strength couldn't be measured in the case of PP and PET substrates. We attribute this difference in shear strength to the fact that the Young's modulus of PET (4.0 GPa[103]) and PP (1.5 GPa[104]) is lower than that of glass (70 GPa[105]), SUS (200 GPa[106]), and Fe (210 GPa[107]), which can cause elastic deformation of PET and PP during bonding and loss of adhesion by restoring forces. These results suggest that the adhesion between **dppz-FLAP1** and the substrate is mainly due to van der Waals forces (Figure 8c).

CONCLUSIONS

In this study, we have pioneered the development of a small-molecule liquid crystalline pressure-sensitive adhesive (LC-PSA) by using an electron-deficient V-shaped dppz-FLAP core as a mesogen. Twofold π-stacking of this core structure induced the shape-assisted self-assembly of a liquid crystalline molecule **dppz-FLAP1**. The packing structure was precisely determined to reveal the formation of a hexagonal columnar LC phase. Remarkably, the LC sample exhibited a good adhesive ability by simple pressing process at room temperature. High shear strength, exceeding 1 MPa, has been achieved with both hydrophilic and hydrophobic glasses, SUS, and Fe substrates, while showing little peel strength and tack stress. The storage modulus of **dppz-FLAP1** was estimated to be ~10^7 Pa, far exceeding the Dahlquist's criterion. The unique feature of the LC-PSA has been revealed in the viscoelastic window of conventional PSAs. Our results indicated that the multiple alkyl chains of **dppz-FLAP1** enhanced both the fluidity and adhesion ability of the material through van der Waals interactions.

This research represents a notable advance in the application of molecular engineering to materials science, moving away from the conventional reliance on hydrogen bonding. Traditionally, liquid crystals have been used to create materials that combine fluidity and ordered structure, but liquid crystals have rarely been applied to cohesive materials. While previous studies have incorporated liquid crystal molecules[69,70,108,109] or liquid crystal polymers[110,111] into adhesives, none of the liquid crystal structures themselves have been reported as pressure-sensitive adhesives. Our approach, which combines strong mesogen interactions with the soft, flexible alkyl chain interactions, not only achieves cohesion but also optimizes wettability for the pressure-sensitive function. This strategy of combining rigid and soft parts shares common principles with other materials such as segmented copolymers,[112] double

network gels,[113] and polymers with dynamic bonding,[114] suggesting a common underlying doctrine in material design. The LC adhesive has a further potential to endow unique LC properties to conventional adhesives, such as an anisotropic shear strength depending on the shear direction and a controllable bonding strength by an electric field.

ASSOCIATED CONTENT

Supporting Information

The Supporting Information is available free of charge on the ACS Publications website.

Experimental detail (PDF)
Movie S1 showing the adhesion process of **dppz-FLAP1** (MP4)

AUTHOR INFORMATION

Corresponding Author

*Shohei Saito - Department of Chemistry, Graduate School of Science, Osaka University, Toyonaka-city, Osaka 560-0043 (Japan); Department of Chemistry, Graduate School of Science, Kyoto University, Sakyo-ku, Kyoto 606-8502 (Japan); Email: saito.shohei@chem.sci.osaka-u.ac.jp

Authors

Kota Ono - Department of Chemistry, Graduate School of Science, Kyoto University, Sakyo-ku, Kyoto 606-8502 (Japan); Department of Chemistry, Graduate School of Science, Osaka University, Toyonaka-city, Osaka 560-0043 (Japan)

Kensuke Suga - Department of Chemistry, Graduate School of Science, Kyoto University, Sakyo-ku, Kyoto 606-8502 (Japan); Department of Chemistry, Graduate School of Science, Osaka University, Toyonaka-city, Osaka 560-0043 (Japan)

Mitsuo Hara - Faculty of Engineering and Design, Kagawa University, Takamatsu-City, Kagawa 761-0396 (Japan)

Katsuki Miyokawa - Department of Chemistry, Graduate School of Science, Kyoto University, Sakyo-ku, Kyoto 606-8502 (Japan)

Tsubasa Honda - Department of Chemistry, Graduate School of Science, Kyoto University, Sakyo-ku, Kyoto 606-8502 (Japan)

Kazuya Otsubo - Graduate School of Science, Tokyo University of Science, Kagurazaka 1-3, Shinjuku-ku, Tokyo 162-8601 (Japan)

Notes

The authors declare no competing financial interest.

ACKNOWLEDGMENT

This work was supported by JST FOREST Program (JPMJFR201L), JSPS KAKENHI (JP21H01917 and JP24H00473), JSPS fellowship (JP22KJ1964), and Iketani Science and Technology Foundation. We thank Prof. Dr. Hideki Yorimitsu, Dr. Junki Ochi, Atsuhiro Ikeno and Prof. Dr. Takuji Hatakeyama (Kyoto Univ.) for their help with high-resolution mass spectrometry measurements. We also thank Prof. Dr. Eriko Sato (Osaka City Univ.) for her help with peeling tests, Prof. Dr. Shigeki Matsunaga (Kyoto Univ.) for helpful discussions, and Dr. Kosuke Higashida (Kyoto Univ.) for his assistance with IGMH analysis.

REFERENCES

(1) Zhao, Y.; Song, S.; Ren, X.; Zhang, J.; Lin, Q.; Zhao, Y. Supramolecular Adhesive Hydrogels for Tissue Engineering Applications. *Chem. Rev.* **2022**, *122* (6), 5604–5640.

(2) Li, W.; Yang, X.; Lai, P.; Shang, L. Bio‐inspired Adhesive Hydrogel for Biomedicine—Principles and Design Strategies. *Smart Med.* **2022**, *1* (1), e20220024.

(3) Liu, Z.; Yan, F. Switchable Adhesion: On-Demand Bonding and Debonding. *Adv. Sci.* **2022**, *9* (12), e2200264.

(4) Fan, H.; Gong, J. P. Bioinspired Underwater Adhesives. *Adv. Mater.* **2021**, *33* (44), e2102983.

(5) Shi, C.-Y.; Zhang, Q.; Tian, H.; Qu, D.-H. Supramolecular Adhesive Materials from Small‐molecule Self‐assembly. *SmartMat.* **2020**, *1* (1), e1012.

(6) Hofman, A. H.; van Hees, I. A.; Yang, J.; Kamperman, M. Bioinspired Underwater Adhesives by Using the Supramolecular Toolbox. *Adv. Mater.* **2018**, *30* (19), 1704640.

(7) Sun, P.; Qin, B.; Xu, J.-F.; Zhang, X. High‐performance Supramolecular Adhesives. *Macromol. Chem. Phys.* **2023**, *224* (3), 2200332.

(8) Heinzmann, C.; Weder, C.; de Espinosa, L. M. Supramolecular Polymer Adhesives: Advanced Materials Inspired by Nature. *Chem. Soc. Rev.* **2016**, *45* (2), 342–358.

(9) Zhang, Q.; Shi, C.-Y.; Qu, D.-H.; Long, Y.-T.; Feringa, B. L.; Tian, H. Exploring a Naturally Tailored Small Molecule for Stretchable, Self-Healing, and Adhesive Supramolecular Polymers. *Sci. Adv.* **2018**, *4* (7), eaat8192.

(10) Liu, H.; Geng, H.; Zhang, X.; Wang, X.; Hao, J.; Cui, J. Hot Melt Super Glue: Multi‐recyclable Polyphenol‐based Supramolecular Adhesives. *Macromol. Rapid Commun.* **2022**, *43* (7), 2100830.

(11) Wang, Z.-H.; Liu, B.-W.; Zeng, F.-R.; Lin, X.-C.; Zhang, J.-Y.; Wang, X.-L.; Wang, Y.-Z.; Zhao, H.-B. Fully Recyclable Multifunctional Adhesive with High Durability, Transparency, Flame Retardancy, and Harsh-Environment Resistance. *Sci. Adv.* **2022**, *8* (50), eadd852.

(12) Li, X.; Deng, Y.; Lai, J.; Zhao, G.; Dong, S. Tough, Long-Term, Water-Resistant, and Underwater Adhesion of Low-Molecular-Weight Supramolecular Adhesives. *J. Am. Chem. Soc.* **2020**, *142* (11), 5371–5379.

(13) Zhang, Q.; Li, T.; Duan, A.; Dong, S.; Zhao, W.; Stang, P. J. Formation of a Supramolecular Polymeric Adhesive via Water-Participant Hydrogen Bond Formation. *J. Am. Chem. Soc.* **2019**, *141* (20), 8058–8063.

(14) Qiao, H.; Wu, B.; Sun, S.; Wu, P. Entropy-Driven Design of Highly Impact-Stiffening Supramolecular Polymer Networks with Salt-Bridge Hydrogen Bonds. *J. Am. Chem. Soc.* **2024**, *146* (11), 7533–7542.

(15) Wu, Z.; Ji, C.; Zhao, X.; Han, Y.; Müllen, K.; Pan, K.; Yin, M. Green-Light-Triggered Phase Transition of Azobenzene Derivatives toward Reversible Adhesives. *J. Am. Chem. Soc.* **2019**, *141* (18), 7385–7390.

(16) Hohl, D. K.; Weder, C. (DE)Bonding on Demand with Optically Switchable Adhesives. *Adv. Opt. Mater.* **2019**, *7* (16), 1900230.

(17) Liu, J.; Tan, C. S. Y.; Scherman, O. A. Dynamic Interfacial Adhesion through Cucurbit[*n*]Uril Molecular Recognition. *Angew. Chem. Int. Ed.* **2018**, *57* (29), 8854–8858.

(18) Heinzmann, C.; Coulibaly, S.; Roulin, A.; Fiore, G. L.; Weder, C. Light-Induced Bonding and Debonding with Supramolecular Adhesives. *ACS Appl. Mater. Interfaces* **2014**, *6* (7), 4713–4719.

(19) Yamaguchi, H.; Kobayashi, Y.; Kobayashi, R.; Takashima, Y.; Hashidzume, A.; Harada, A. Photoswitchable Gel Assembly Based on Molecular Recognition. *Nat. Commun.* **2012**, *3* (1), 1–5.
(20) Liu, X.; Zhang, Q.; Gao, G. Bioinspired Adhesive Hydrogels Tackified by Nucleobases. *Adv. Funct. Mater.* **2017**, *27* (44), 1703132.
(21) Liu, Y.; Meng, H.; Konst, S.; Sarmiento, R.; Rajachar, R.; Lee, B. P. Injectable Dopamine-Modified Poly(Ethylene Glycol) Nanocomposite Hydrogel with Enhanced Adhesive Property and Bioactivity. *ACS Appl. Mater. Interfaces* **2014**, *6* (19), 16982–16992.
(22) Wu, S.; Cai, C.; Li, F.; Tan, Z.; Dong, S. Deep Eutectic Supramolecular Polymers: Bulk Supramolecular Materials. *Angew. Chem. Int. Ed.* **2020**, *59* (29), 11871–11875.
(23) Ji, X.; Ahmed, M.; Long, L.; Khashab, N. M.; Huang, F.; Sessler, J. L. Adhesive Supramolecular Polymeric Materials Constructed from Macrocycle-Based Host-Guest Interactions. *Chem. Soc. Rev.* **2019**, *48* (10), 2682–2697.
(24) Liu, J.; Scherman, O. A. Cucurbit[*n*]Uril Supramolecular Hydrogel Networks as Tough and Healable Adhesives. *Adv. Funct. Mater.* **2018**, *28* (21), 1800848.
(25) Nakamura, T.; Takashima, Y.; Hashidzume, A.; Yamaguchi, H.; Harada, A. A Metal–Ion-Responsive Adhesive Material via Switching of Molecular Recognition Properties. *Nat. Commun.* **2014**, *5* (1), 1–9.
(26) Nakahata, M.; Takashima, Y.; Yamaguchi, H.; Harada, A. Redox-Responsive Self-Healing Materials Formed from Host–Guest Polymers. *Nat. Commun.* **2011**, *2* (1), 1–6.
(27) Jian, J.; Zhou, Y.; Su, J.; Gao, Z.; Wei, S.; Han, S. Supramolecular Adhesive Materials Based on Urea Assembly. *Chem. Eng. J.* **2024**, *480*, 148061.
(28) Chen, H.; Liu, X.; He, Q.; Zhang, S.; Xu, S.; Wang, Y.-Z. Upcycling Waste Thermosetting Polyimide Resins into High‐performance and Sustainable Low‐temperature‐resistance Adhesives. *Adv. Mater.* **2024**, *36*, 2310779.
(29) Chen, S.; Zhang, K.; Li, Z.; Wu, Y.; Zhu, B.; Zhu, J. Hydrogen-Bonded Supramolecular Adhesives: Synthesis, Responsiveness, and Application. *Supramolecular Materials* **2023**, *2*, 100032.
(30) Chen, S.; Li, Z.; Wu, Y.; Mahmood, N.; Lortie, F.; Bernard, J.; Binder, W. H.; Zhu, J. Hydrogen‐bonded Supramolecular Polymer Adhesives: Straightforward Synthesis and Strong Substrate Interaction. *Angew. Chem. Int. Ed.* **2022**, *61* (27), e202203876.
(31) Sun, P.; Li, Y.; Qin, B.; Xu, J.-F.; Zhang, X. Super Strong and Multi-Reusable Supramolecular Epoxy Hot Melt Adhesives. *ACS Mater. Lett.* **2021**, *3* (7), 1003–1009.
(32) Wu, S.; Cai, C.; Li, F.; Tan, Z.; Dong, S. Supramolecular Adhesive Materials from Natural Acids and Sugars with Tough and Organic Solvent-Resistant Adhesion. *CCS Chem.* **2021**, *3* (6), 1690–1700.
(33) Li, X.; Wang, Z.; Li, W.; Sun, J. Superstrong Water-Based Supramolecular Adhesives Derived from Poly(Vinyl Alcohol)/Poly(Acrylic Acid) Complexes. *ACS Mater. Lett.* **2021**, *3* (6), 875–882.
(34) Courtois, J.; Baroudi, I.; Nouvel, N.; Degrandi, E.; Pensec, S.; Ducouret, G.; Chanéac, C.; Bouteiller, L.; Creton, C. Supramolecular Soft Adhesive Materials. *Adv. Funct. Mater.* **2010**, *20* (11), 1803–1811.
(35) Yamauchi, K.; Lizotte, J. R.; Long, T. E. Thermoreversible Poly(Alkyl Acrylates) Consisting of Self-Complementary Multiple Hydrogen Bonding. *Macromolecules* **2003**, *36* (4), 1083–1088.
(36) Miyamoto, Y.; Watabe, K.; Amano, Y.; Imai, T.; Osaki, H. Photomelt and Photoinduced Tacky Resins Comprising Disulfide and Photoinitiators as Easy-to-Release, Pressure-Sensitive, and Separator-Free Adhesives. *Chem. Eng. J.* **2023**, *471* (144109), 144109.
(37) Liu, J.; Huang, Y.-S.; Liu, Y.; Zhang, D.; Koynov, K.; Butt, H.-J.; Wu, S. Reconfiguring Hydrogel Assemblies Using a Photocontrolled Metallopolymer Adhesive for Multiple Customized Functions. *Nat. Chem.* **2024**, 1–10.
(38) Ke, X.; Tang, S.; Dong, Z.; Ren, K.; Yu, P.; Xu, X.; Yang, J.; Luo, J.; Li, J. An Instant, Repeatable and Universal Supramolecular Adhesive Based on Natural Small Molecules for Dry/Wet Environments. *Chem. Eng. J.* **2022**, *442*, 136206.
(39) Sun, P.; Mei, S.; Xu, J.-F.; Zhang, X. A Bio‐based Supramolecular Adhesive: Ultra‐high Adhesion Strengths at Both Ambient and Cryogenic Temperatures and Excellent Multi‐reusability. *Adv. Sci.* **2022**, *9* (28), 2203182.
(40) Wang, Z.; Huang, K.; Wan, X.; Liu, M.; Chen, Y.; Shi, X.; Wang, S. High‐strength plus Reversible Supramolecular Adhesives Achieved by Regulating Intermolecular $Pt^{II}\cdots Pt^{II}$ Interactions. *Angew. Chem. Int. Ed.* **2022**, *61* (40), e202211495.
(41) Liang, Y.; Wang, K.; Li, J.; Zhang, Y.; Liu, J.; Zhang, K.; Cui, Y.; Wang, M.; Liu, C.-S. Low-Molecular-Weight Supramolecular Adhesives Based on Non-Covalent Self-Assembly of a Small Molecular Gelator. *Mater. Horiz.* **2022**, *9* (6), 1700–1707.
(42) Guan, W.; Jiang, W.; Deng, X.; Tao, W.; Tang, J.; Li, Y.; Peng, J.; Chen, C.-L.; Liu, K.; Fang, Y. Supramolecular Adhesives with Extended Tolerance to Extreme Conditions via Water‐modulated Noncovalent Interactions. *Angew. Chem. Int. Ed.* **2023**, *62* (23), e202303506.
(43) Brubaker, C. E.; Messersmith, P. B. Enzymatically Degradable Mussel-Inspired Adhesive Hydrogel. *Biomacromolecules* **2011**, *12* (12), 4326–4334.
(44) North, M. A.; Del Grosso, C. A.; Wilker, J. J. High Strength Underwater Bonding with Polymer Mimics of Mussel Adhesive Proteins. *ACS Appl. Mater. Interfaces* **2017**, *9* (8), 7866–7872.
(45) Liu, Y.; Meng, H.; Messersmith, P. B.; Lee, B. P.; Dalsin, J. L. Biomimetic Adhesives and Coatings Based on Mussel Adhesive Proteins. In *Biological Adhesives*; Springer International Publishing: Cham, 2016; pp 345–378.
(46) Ahn, B. K.; Das, S.; Linstadt, R.; Kaufman, Y.; Martinez-Rodriguez, N. R.; Mirshafian, R.; Kesselman, E.; Talmon, Y.; Lipshutz, B. H.; Israelachvili, J. N.; Waite, J. H. High-Performance Mussel-Inspired Adhesives of Reduced Complexity. *Nat. Commun.* **2015**, *6* (1), 1–7.
(47) Liu, K.; Wu, P. Small Ionic‐liquid‐based Molecule Drives Strong Adhesives. *Angew. Chem. Int. Ed.* **2024**, e202403220.
(48) Zhang, J.; Wang, W.; Zhang, Y.; Wei, Q.; Han, F.; Dong, S.; Liu, D.; Zhang, S. Small-Molecule Ionic Liquid-Based Adhesive with Strong Room-Temperature Adhesion Promoted by Electrostatic Interaction. *Nat. Commun.* **2022**, *13* (1), 1–10.
(49) Sikder, A.; Esen, C.; O'Reilly, R. K. Nucleobase-Interaction-Directed Biomimetic Supramolecular Self-Assembly. *Acc. Chem. Res.* **2022**, *55* (12), 1609–1619.
(50) Tian, Y.; Wu, J.; Fang, X.; Guan, L.; Yao, N.; Yang, G.; Wang, Z.; Hua, Z.; Liu, G. Rational Design of Bioinspired Nucleobase‐containing Polymers as Tough Bioplastics and Ultra‐strong Adhesives. *Adv. Funct. Mater.* **2022**, *32* (14), 2112741.
(51) Mazzotta, M. G.; Putnam, A. A.; North, M. A.; Wilker, J. J. Weak Bonds in a Biomimetic Adhesive Enhance Toughness and Performance. *J. Am. Chem. Soc.* **2020**, *142* (10), 4762–4768.
(52) *Handbook of Liquid Crystals*, 2nd ed.; Goodby, J. W., Collings, P. J., Kato, T., Tschierske, C., Gleeson, H., Raynes, P., Eds.; Wiley-VCH Verlag: Weinheim, Germany, 2014.
(53) Uchida, J.; Soberats, B.; Gupta, M.; Kato, T. Advanced Functional Liquid Crystals. *Adv. Mater.* **2022**, *34* (23), 2109063.
(54) Fleischmann, E.-K.; Zentel, R. Liquid‐crystalline Ordering as a Concept in Materials Science: From Semiconductors to Stimuli‐responsive Devices. *Angew. Chem. Int. Ed.* **2013**, *52* (34), 8810–8827.

(55) Shoji, Y.; Komiyama, R.; Kobayashi, M.; Kosaka, A.; Kajitani, T.; Haruki, R.; Kumai, R.; Adachi, S.-I.; Tada, T.; Karasawa, N.; Nakano, H.; Nakamura, H.; Sakurai, H.; Fukushima, T. Collective Bending Motion of a Two-Dimensionally Correlated Bowl-Stacked Columnar Liquid Crystalline Assembly under a Shear Force. *Sci. Adv.* **2023**, *9* (19), eadg8202.

(56) Rosen, B. M.; Wilson, C. J.; Wilson, D. A.; Peterca, M.; Imam, M. R.; Percec, V. Dendron-Mediated Self-Assembly, Disassembly, and Self-Organization of Complex Systems. *Chem. Rev.* **2009**, *109* (11), 6275–6540.

(57) Saito, S.; Nobusue, S.; Tsuzaka, E.; Yuan, C.; Mori, C.; Hara, M.; Seki, T.; Camacho, C.; Irle, S.; Yamaguchi, S. Light-Melt Adhesive Based on Dynamic Carbon Frameworks in a Columnar Liquid-Crystal Phase. *Nat. Commun.* **2016**, *7* (1), 12094.

(58) Woods, J. F.; Gallego, L.; Maisch, A.; Renggli, D.; Cuocci, C.; Blacque, O.; Steinfeld, G.; Kaech, A.; Spingler, B.; Vargas Jentzsch, A.; Rickhaus, M. Saddles as Rotational Locks within Shape-Assisted Self-Assembled Nanosheets. *Nat. Commun.* **2023**, *14* (1), 4725.

(59) Woods, J. F.; Gallego, L.; Pfister, P.; Maaloum, M.; Vargas Jentzsch, A.; Rickhaus, M. Shape-Assisted Self-Assembly. *Nat. Commun.* **2022**, *13* (1), 1–8.

(60) Kato, K.; Takaba, K.; Maki-Yonekura, S.; Mitoma, N.; Nakanishi, Y.; Nishihara, T.; Hatakeyama, T.; Kawada, T.; Hijikata, Y.; Pirillo, J.; Scott, L. T.; Yonekura, K.; Segawa, Y.; Itami, K. Double-Helix Supramolecular Nanofibers Assembled from Negatively Curved Nanographenes. *J. Am. Chem. Soc.* **2021**, *143* (14), 5465–5469.

(61) Hada, M.; Saito, S.; Tanaka, S.; Sato, R.; Yoshimura, M.; Mouri, K.; Matsuo, K.; Yamaguchi, S.; Hara, M.; Hayashi, Y.; Röhricht, F.; Herges, R.; Shigeta, Y.; Onda, K.; Miller, R. J. D. Structural Monitoring of the Onset of Excited-State Aromaticity in a Liquid Crystal Phase. *J. Am. Chem. Soc.* **2017**, *139* (44), 15792–15800.

(62) Mouri, K.; Saito, S.; Yamaguchi, S. Highly Flexible Π‐expanded Cyclooctatetraenes: Cyclic Thiazole Tetramers with Head‐to‐tail Connection. *Angew. Chem. Int. Ed.* **2012**, *51* (24), 5971–5975.

(63) Mizuno, H.; Nakazawa, H.; Harada, M.; Yakiyama, Y.; Sakurai, H.; Fukuhara, G. Sumanene-Stacked Supramolecular Polymers. Dynamic, Solvation-Directed Control. *Chem. Commun.* **2023**, *59* (63), 9595–9598.

(64) Furukawa, S.; Wu, J.; Koyama, M.; Hayashi, K.; Hoshino, N.; Takeda, T.; Suzuki, Y.; Kawamata, J.; Saito, M.; Akutagawa, T. Ferroelectric Columnar Assemblies from the Bowl-to-Bowl Inversion of Aromatic Cores. *Nat. Commun.* **2021**, *12* (1), 1–9.

(65) Renner, R.; Stolte, M.; Würthner, F. Self-Assembly of Bowl-Shaped Naphthalimide-Annulated Corannulene. *ChemistryOpen* **2020**, *9* (1), 32–39.

(66) Kang, J.; Miyajima, D.; Mori, T.; Inoue, Y.; Itoh, Y.; Aida, T. A Rational Strategy for the Realization of Chain-Growth Supramolecular Polymerization. *Science* **2015**, *347* (6222), 646–651.

(67) Martinez, C. R.; Iverson, B. L. Rethinking the Term "Pi-Stacking." *Chem. Sci.* **2012**, *3* (7), 2191.

(68) Huang, X.; Shangguan, Z.; Zhang, Z.-Y.; Yu, C.; He, Y.; Fang, D.; Sun, W.; Li, Y.-C.; Yuan, C.; Wu, S.; Li, T. Visible-Light-Induced Reversible Photochemical Crystal–Liquid Transitions of Azo-Switches for Smart and Robust Adhesives. *Chem. Mater.* **2022**, *34* (6), 2636–2644.

(69) Koike, M.; Aizawa, M.; Minamikawa, H.; Shishido, A.; Yamamoto, T. Photohardenable Pressure-Sensitive Adhesives Using Poly(Methyl Methacrylate) Containing Liquid Crystal Plasticizers. *ACS Appl. Mater. Interfaces* **2021**, *13* (33), 39949–39956.

(70) Koike, M.; Aizawa, M.; Akamatsu, N.; Shishido, A.; Matsuzawa, Y.; Yamamoto, T. Photoplasticization Behavior and Photoinduced Pressure-Sensitive Adhesion Properties of Various Polymers Containing an Azobenzene-Doped Liquid Crystal. *Bull. Chem. Soc. Jpn.* **2020**, *93* (12), 1588–1594.

(71) Ito, S.; Akiyama, H.; Sekizawa, R.; Mori, M.; Yoshida, M.; Kihara, H. Light-Induced Reworkable Adhesives Based on ABA-Type Triblock Copolymers with Azopolymer Termini. *ACS Appl. Mater. Interfaces* **2018**, *10* (38), 32649–32658.

(72) Zhou, H.; Xue, C.; Weis, P.; Suzuki, Y.; Huang, S.; Koynov, K.; Auernhammer, G. K.; Berger, R.; Butt, H.-J.; Wu, S. Photoswitching of Glass Transition Temperatures of Azobenzene-Containing Polymers Induces Reversible Solid-to-Liquid Transitions. *Nat. Chem.* **2017**, *9* (2), 145–151.

(73) Akiyama, H.; Yoshida, M. Photochemically Reversible Liquefaction and Solidification of Single Compounds Based on a Sugar Alcohol Scaffold with Multi Azo‐arms. *Adv. Mater.* **2012**, *24* (17), 2353–2356.

(74) Creton, C. Pressure-Sensitive Adhesives: An Introductory Course. *MRS Bull.* **2003**, *28* (6), 434–439.

(75) Mapari, S.; Mestry, S.; Mhaske, S. T. Developments in Pressure-Sensitive Adhesives: A Review. *Polym. Bull.* **2021**, *78* (7), 4075–4108.

(76) Deng, X. Progress on Rubber-Based Pressure-Sensitive Adhesives. *The Journal of Adhesion* **2018**, *94* (2), 77–96.

(77) Sun, S.; Li, M.; Liu, A. A Review on Mechanical Properties of Pressure Sensitive Adhesives. *Int. J. Adhes. Adhes.* **2013**, *41*, 98–106.

(78) Khan, I.; Poh, B. T. Natural Rubber-Based Pressure-Sensitive Adhesives: A Review. *J Polym Environ* **2011**, *19* (3), 793–811.

(79) Dikshit, K. V.; Visal, A. M.; Janssen, F.; Larsen, A.; Bruns, C. J. Pressure-Sensitive Supramolecular Adhesives Based on Lipoic Acid and Biofriendly Dynamic Cyclodextrin and Polyrotaxane Cross-Linkers. *ACS Appl. Mater. Interfaces* **2023**, *15* (13), 17256–17267.

(80) Lin, H.; Chen, H.; Liu, J.; Li, H.; Mao, D. Towards Sturdy and Sensable Pressure-Sensitive Adhesive through Hierarchical Supramolecular Interaction. *Supramolecular Materials* **2023**, *2*, 100047.

(81) Gao, S.; Wang, W.; Wu, T.; Jiang, S.; Qi, J.; Zhu, Z.; Zhang, B.; Huang, J.; Yan, Y. Folic Acid-Based Coacervate Leading to a Double-Sided Tape for Adhesion of Diverse Wet and Dry Substrates. *ACS Appl. Mater. Interfaces* **2021**, *13* (29), 34843–34850.

(82) Callies, X.; Herscher, O.; Fonteneau, C.; Robert, A.; Pensec, S.; Bouteiller, L.; Ducouret, G.; Creton, C. Combined Effect of Chain Extension and Supramolecular Interactions on Rheological and Adhesive Properties of Acrylic Pressure-Sensitive Adhesives. *ACS Appl. Mater. Interfaces* **2016**, *8* (48), 33307–33315.

(83) Yuan, C.; Saito, S.; Camacho, C.; Irle, S.; Hisaki, I.; Yamaguchi, S. A π-Conjugated System with Flexibility and Rigidity That Shows Environment-Dependent RGB Luminescence. *J. Am. Chem. Soc.* **2013**, *135* (24), 8842–8845.

(84) Yuan, C.; Saito, S.; Camacho, C.; Kowalczyk, T.; Irle, S.; Yamaguchi, S. Hybridization of a Flexible Cyclooctatetraene Core and Rigid Aceneimide Wings for Multiluminescent Flapping π Systems. *Chem. Eur. J* **2014**, *20* (8), 2193–2200.

(85) Zhang, Y.; Zhang, J.; Shi, C.; Sun, N.; Wang, Q. Dipyrido[3,2-a:2′,3′-c]Phenazine Acceptor Based Thermally Activated Delayed Fluorescence Emitters. *Dyes Pigm.* **2022**, *206*, 110634.

(86) Choudhury, R. R.; Chitra, R. Stacking Interaction between Homostacks of Simple Aromatics and the Factors Influencing These Interactions. *CrystEngComm* **2010**, *12* (7), 2113.

(87) Tobe, Y.; Utsumi, N.; Kawabata, K.; Nagano, A.; Adachi, K.; Araki, S.; Sonoda, M.; Hirose, K.; Naemura, K. M-Diethynylbenzene Macrocycles: Syntheses and Self-

Association Behavior in Solution. *J. Am. Chem. Soc.* **2002**, *124* (19), 5350–5364.
(88) Hunter, C. A.; Sanders, J. K. M. The Nature of .Pi.-.Pi. Interactions. *J. Am. Chem. Soc.* **1990**, *112* (14), 5525–5534.
(89) Suga, K.; Yamakado, T.; Saito, S. Dual Ratiometric Fluorescence Monitoring of Mechanical Polymer Chain Stretching and Subsequent Strain-Induced Crystallization. *J. Am. Chem. Soc.* **2023**, *145* (49), 26799–26809.
(90) Yamakado, T.; Saito, S. Ratiometric Flapping Force Probe That Works in Polymer Gels. *J. Am. Chem. Soc.* **2022**, *144* (6), 2804–2815.
(91) Suga, K.; Yamakado, T.; Saito, S. Nitrogen-Substitution in the Flapping Wings of Cyclooctatetraene-Fused Molecules. *Bull. Chem. Soc. Jpn* **2021**, *94* (7), 1999‑2002.
(92) Greguric, A.; Greguric, I. D.; Hambley, T. W.; Aldrich-Wright, J. R.; Collins, J. G. Minor Groove Intercalation of Δ-[Ru(Me2phen)2dppz]2+ to the Hexanucleotide d(GTCGAC)2. *J. Chem. Soc., Dalton Trans.* **2002**, No. 6, 849.
(93) Rietveld, H. M. A Profile Refinement Method for Nuclear and Magnetic Structures. *J. Appl. Crystallogr.* **1969**, *2* (2), 65–71.
(94) Lu, T.; Chen, Q. Independent Gradient Model Based on Hirshfeld Partition: A New Method for Visual Study of Interactions in Chemical Systems. *J. Comput. Chem.* **2022**, *43* (8), 539–555.
(95) Shoji, Y.; Kobayashi, M.; Kosaka, A.; Haruki, R.; Kumai, R.; Adachi, S.-I.; Kajitani, T.; Fukushima, T. Design of Discotic Liquid Crystal Enabling Complete Switching along with Memory of Homeotropic and Homogeneous Alignment over a Large Area. *Chem. Sci.* **2022**, *13* (34), 9891–9901.
(96) Tordjeman, P.; Papon, E.; Villenave, J.-J. Tack Properties of Pressure‐sensitive Adhesives. *J. Polym. Sci. B Polym. Phys.* **2000**, *38* (9), 1201–1208.
(97) Dahlquist, C. A. An Investigation into the Nature of Tack. *Adhes. Age* **1959**, *2*, 25–29.
(98) Chang, E. P. Viscoelastic Windows of Pressure-Sensitive Adhesives. *The Journal of Adhesion* **1991**, *34* (1–4), 189–200.
(99) Hwang, C.; Shin, S.; Ahn, D.; Paik, H.-J.; Lee, W.; Yu, Y. Realizing Cross-Linking-Free Acrylic Pressure-Sensitive Adhesives with Intensive Chain Entanglement through Visible-Light-Mediated Photoiniferter-Reversible Addition–Fragmentation Chain-Transfer Polymerization. *ACS Appl. Mater. Interfaces* **2023**, *15* (50), 58905–58916.
(100) Engelen, S.; Droesbeke, M.; Aksakal, R.; Du Prez, F. E. Ring-Opening Metathesis Polymerization for the Synthesis of Terpenoid-Based Pressure-Sensitive Adhesives. *ACS Macro Lett.* **2022**, *11* (12), 1378–1383.
(101) Fuensanta, M.; Martin-Martínez, J. M. Thermoplastic Polyurethane Pressure Sensitive Adhesives Made with Mixtures of Polypropylene Glycols of Different Molecular Weights. *Int. J. Adhes. Adhes.* **2019**, *88*, 81–90.
(102) Choi, B.; Kim, J. W.; Choi, G.; Jeong, S.; Choi, E.; Kim, H. Grafting Self-Immolative Poly(Benzyl Ether)s toward Sustainable Adhesive Thermosets with Reversible Bonding and Triggered de-Bonding Capabilities. *J. Mater. Chem. A Mater. Energy Sustain.* **2023**, *11* (20), 10538–10544.
(103) *Determination of Young's Modulus of PET Sheets from Lamb Wave Velocity Measurement*.
(104) Serra-Parareda, F.; Tarrés, Q.; Espinach, F. X.; Vilaseca, F.; Mutjé, P.; Delgado-Aguilar, M. Influence of Lignin Content on the Intrinsic Modulus of Natural Fibers and on the Stiffness of Composite Materials. *Int. J. Biol. Macromol.* **2020**, *155*, 81–90.
(105) Shen, Y.; Zhang, Z.; Fukuda, T. Bending Spring Rate Investigation of Nanopipette for Cell Injection. *Nanotechnology* **2015**, *26* (15), 155702.
(106) Kubota, K.; Ueda, M.; Nakagawa, H. Effect of Prior Austenite Grain Size on Yielding Behavior of the Low-C Martensitic Stainless Steel. *Mater. Sci. For.* **2016**, *879*, 1031–1035.
(107) Strizhalo, V. A.; Voitenko, A. F. Elastic Characteristics of Iron-Glass Materials at Low Temperatures. *Strength Mater.* **1998**, *30* (1), 31–35.
(108) Zheng, J.; Zong, Y.; Zhao, G.; Yu, Z.; Wang, M.; Zhu, C.; Li, C.; Liu, J.; Gui, D. Nematic Liquid Crystal 4-Cyano-4′-Pentylbiphenyl Functionalization of MWNTs for Improved Thermal and Mechanical Properties of Silicone Pressure Sensitive Adhesives. *Int. J. Adhes. Adhes.* **2020**, *98*, 102457.
(109) Yamamoto, T.; Hasegawa, R.; Kawata, Y.; Kihara, H.; Naga, N. Photoplasticization Effect of an Azobenzene-Doped Liquid Crystal Depending on Phase Structures. *Chem. Lett.* **2018**, *47* (3), 272–275.
(110) Annapooranan, R.; Suresh Jeyakumar, S.; J. Chambers, R.; Long, R.; Cai, S. Ultra Rate‐dependent Pressure Sensitive Adhesives Enabled by Soft Elasticity of Liquid Crystal Elastomers. *Adv. Funct. Mater.* **2024**, *34* (1), 2309123.
(111) Lou, P.; Li, X.; Yao, M.; Nie, J.; He, Y. Thermal Debonding Pressure-Sensitive Adhesive Blended with Liquid Crystal Polymers. *Prog. Org. Coat.* **2023**, *185*, 107932.
(112) Noshay, A.; Mcgrath, E. J. *Block Copolymers – Overview and Critical Survey*; Academic Press Inc., 1971.
(113) Gong, J. P. Why Are Double Network Hydrogels so Tough? *Soft Matter* **2010**, *6* (12), 2583.
(114) Wang, S.; Hu, Y.; Kouznetsova, T. B.; Sapir, L.; Chen, D.; Herzog-Arbeitman, A.; Johnson, J. A.; Rubinstein, M.; Craig, S. L. Facile Mechanochemical Cycloreversion of Polymer Cross-Linkers Enhances Tear Resistance. *Science* **2023**, *380* (6651), 1248–1252.

Table of Contents artwork